

The Orbit and Mass of the Sagittarius Dwarf Galaxy

Ing-Guey Jiang and James Binney

Theoretical Physics, University of Oxford, Oxford, OX1 3NP

ABSTRACT

Possible orbital histories of the Sgr dwarf galaxy are explored. A special-purpose N -body code is used to construct the first models of the Milky Way – Sgr Dwarf system in which both the Milky Way and the Sgr Dwarf are represented by full N -body systems and followed for a Hubble time. These models are used to calibrate a semi-analytic model of the Dwarf’s orbit that enable us to explore a wider parameter space than is accessible to the N -body models. We conclude that the extant data on the Dwarf are compatible with a wide range of orbital histories. At one extreme the Dwarf initially possesses $\sim 10^{11} M_{\odot}$ and starts from a Galactocentric distance $R_{\text{D}}(0) \gtrsim 200$ kpc. At the other extreme the Dwarf starts with $\sim 10^9 M_{\odot}$ and $R_{\text{D}}(0) \sim 60$ kpc, similar to its present apocentric distance. In all cases the Dwarf is initially dark-matter dominated and the current velocity dispersion of the Dwarf’s dark matter is tightly constrained to be $(21 \pm 2) \text{ km s}^{-1}$. This number is probably compatible with the smaller measured dispersion of the Dwarf’s stars because of (a) the dynamical difference between dark and luminous matter, and (b) velocity anisotropy.

Key words: Galaxy: kinematics and dynamics – Galaxy: halo – galaxies: individual: Sgr Dwarf – galaxies: dwarf – galaxies: formation

INTRODUCTION

The Milky Way’s nearest neighbour, the Sagittarius dwarf galaxy, lies only 16 kpc from the Galactic centre, but was until 1993 hidden from us by the inner Milky Way. Since the discovery of this object by Ibata et al. (1994), several studies have explored its extent on the sky, its mean radial velocity, its proper motion perpendicular to the Galactic plane, and its internal velocity dispersion (Ibata et al. 1997). The data currently in hand constrain the present orbit of the Dwarf quite tightly. Ibata & Lewis (1998) find that acceptable orbits have periods $\lesssim 1$ Gyr and are moderately eccentric, with apocentres near 60 kpc and pericentres near 20 kpc.

Moving on its orbit the Dwarf is subject to significant tidal distortion by the Milky Way. Indeed, the observed elongation of the Dwarf perpendicular to the Galactic plane is thought to be the result of tidal shear. In this context it is important to understand how the Dwarf has avoided being torn apart by Galactic tides. Velásquez & White (1995), Johnson et al. (1995) and Ibata & Lewis (1998) have studied this problem and concluded that there is at most a tight corner of parameter space in which the Dwarf could have survived to the present time. Specifically, if light is assumed to trace mass, survival is impossible: to ensure survival it is essential to pack as much mass as possible within the observed outer radius, r_t , of the Dwarf.

The observed internal velocity dispersion places an upper limit on the Dwarf’s central mass density, so to maximize the Dwarf’s mass one has to pack the material around Dwarf’s edge. Hence the extra mass must be dark and within the Dwarf’s outer limit its density must decrease outwards as slowly as possible. Since material beyond the

tidal radius is not bound to the Dwarf, the density of dark matter should plummet near r_t . Ibata & Lewis found a density distribution that was consistent with these requirements and has a non-negative distribution function $f(E)$: $\rho(r) \propto (e^{-(r/1 \text{ kpc})^2} - e^{-1})$. They present N -body simulations of this dark-matter distribution moving on the Dwarf’s orbit, and show that it is torn apart by the Galaxy on an acceptably long timescale.

The model of Ibata & Lewis is attractive because we know that dark matter contributes significantly to the potentials of dwarf galaxies. It is, however, finely tuned in that both the density and the radial extent of the dark-matter distribution can be neither larger nor smaller than the chosen values. This fine tuning would not detract from the plausibility of the model if it arose naturally as the Dwarf’s orbit and the density profile were fashioned by Galactic tides and dynamical friction against the Galactic halo. In this paper we present simulations designed to investigate this question.

Specifically, we aim to find initial configurations in which the Dwarf’s halo encompasses a conventional flat-rotation-curve section in addition to a homogeneous core. We wish to simulate the stripping of this halo to leave the sharp-edged homogeneous rump envisaged by Ibata & Lewis. Full N -body simulations of this process are extremely costly because the Galaxy’s dark halo has to be simulated out to a Galactocentric radius $r \gtrsim 250$ kpc, within which its mass is $\sim 2 \times 10^{12} M_{\odot}$, while simultaneously following the internal dynamics of the Dwarf, which now contains $\lesssim 10^8 M_{\odot}$ of visible material and probably a comparable amount of dark matter. Resolution of the visible Dwarf into $\gtrsim 100$ particles, implies that individual particles have

masses $\sim 10^6 M_\odot$, so $\gtrsim 2 \times 10^6$ such particles are required to represent the Galactic halo. This large number of particles has to be followed for a Hubble time, or ~ 400 current half-light crossing times of the Dwarf. In principle one may represent the Galactic halo by fewer particles of higher mass, but this strategy is unsafe because in such a simulation two-particle relaxation proceeds rapidly and artificially accelerates the disruption of the Dwarf, which is a process of prime interest.

Previous simulations of the Dwarf's orbit have relied on a number of more-or-less unsatisfactory work-arounds, such as treating the Galactic potential as fixed, and possibly augmented by dynamical friction (Velásquez & White 1995, Johnston et al. 1995, Ibata & Lewis 1998), studying only orbits that never reach far out into the Galactic halo and using more massive particles for the halo than for the Dwarf (Gómez-Flechoso, Fux & Martinet, 1999). Our strategy has been two-fold. First we have tailored a potential solver to the problem: this uses two multipole expansions, one centred on the Galactic centre and one centred on the Dwarf. Second we have used a small number of large N -body simulations to calibrate semi-analytic calculations that include dynamical friction and tidal stripping, and have used the semi-analytic calculations to explore more thoroughly the parameter space associated with the initial Dwarf and its orbit.

The paper is organized as follows. Section 2 summarizes the mass profiles assumed for the Milky Way and the Dwarf. Section 3 describes the N -body code that was tailored to the problem, together with tests of the code and three full N -body models of the Galaxy–Dwarf system. Section 4 describes a semi-analytic model calibrated by reference to the N -body models. Section 5 sums up and discusses the observable consequences of extensive mass loss by the Dwarf.

INITIAL CONDITIONS

To be possessed of an extensive halo, the Dwarf must initially be at a much larger Galactocentric radius than at present. Hence the orbit must initially have had a large apocentre, and therefore have been a long-period orbit. Since we know that the Dwarf is now on a short-period orbit, it must have lost significant orbital energy. Zhao (1998) suggested that a close encounter with the Magellanic Clouds could have led to this loss of orbital energy. This possibility seems unlikely, however, because the gravitational field of the Clouds is probably too weak to deflect the Dwarf through a significant angle, given the relative velocity ($\sim 300 \text{ km s}^{-1}$) at which the Dwarf would have encountered the Clouds – see the simulations of Ibata & Lewis for support of this view. Given our belief that the Dwarf will initially have possessed an extensive dark halo, the natural mechanism for loss of orbital energy is dynamical friction.

If the dark-halo model of Ibata & Lewis is correct, the current mass of the Dwarf is $\sim 10^9 M_\odot$. Dynamical friction against the Galactic halo has only a modest effect on a body of this mass. For example, by equation (7-27) of Binney & Tremaine (1987; hereafter BT), its decay time from a circular orbit of initial radius 30 kpc is $(50/\ln \Lambda)$ Gyr with $\ln \Lambda \sim 8$ (see below), and increases as the square of the initial radius. Hence, if the mass of the Dwarf were initially as small as it now probably is, its orbit would not have evolved

very much, and it could never have possessed a generic dark halo.

If, by contrast, the Dwarf started out much more massive, its orbit could have evolved from the large galactocentric radius. At such a large radius it could have possessed the extensive halo that alone would make it massive. Hence, it is a priori plausible that there are a number of self-consistent solutions for the Dwarf's past: at one extreme it was from the outset severely tidally truncated and has moved at all times on the same short-period orbit; at the other extreme, it was initially possessed of a massive power-law halo that caused it to sink rapidly inwards under the influence of dynamical friction, and be progressively stripped of its halo. Ibata & Lewis have presented an orbit of the first kind. We seek orbits of the second kind.

Initial density profiles and velocities

The Galactic disk is assumed to be rigid. The surface density of the disk is taken to be exponential inside $R_t = 19.75$ kpc and then to fall rapidly to zero by $R_0 = 20$ kpc. In terms of the variable

$$x \equiv \frac{\pi}{2} \frac{R - R_r}{R_0 - R_t}, \quad (1a)$$

the disk's surface density is given by

$$\Sigma(R) = \Sigma_0 e^{-R/R_d} \times \begin{cases} 1 & x \leq 0 \\ \cos^2 x & 0 < x \leq \pi/2 \\ 0 & \text{otherwise.} \end{cases} \quad (1b)$$

We set the disk's scale-length to $R_d = 3.4$ kpc, which yields a halo-dominated rotation curve (Dehnen & Binney 1997). The parameter Σ_0 is set such that the disk's total mass is $10^{11} M_\odot$.

Flat rotation curves imply that dark halos have approximately isothermal density profiles. Therefore we assume that the initial density profiles of both the Dwarf and the Milky Way are given by

$$\rho(r) = \begin{cases} \frac{v_c^2}{4\pi G} \frac{e^{-r/r_0}}{r^2 + r_c^2} & \text{for } r \leq r_\infty \\ 0 & \text{otherwise.} \end{cases} \quad (2)$$

Table 1 gives values for the Galaxy of the parameters v_c , r_c , r_0 and r_∞ . These values are chosen to ensure that the rotation curve is compatible with observations (Dehnen & Binney, 1997) and that the mass of the Local Group is as large as the timing argument implies (e.g., Schmoldt & Saha, 1998). Fig. 1 shows the overall circular-speed curve and its contributions from disk and halo.

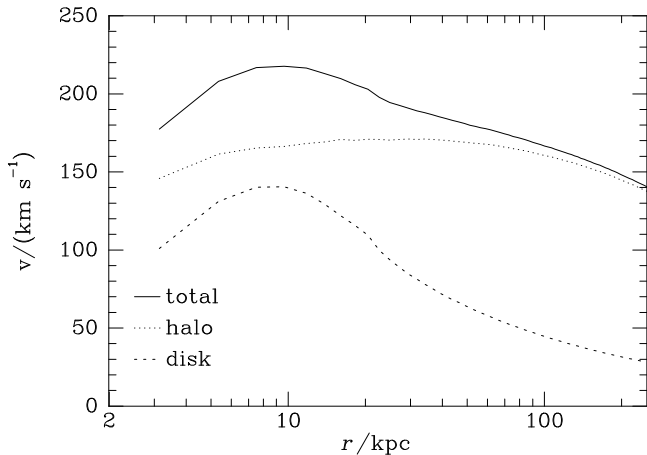
The Dwarf's core radius is taken to be $r_c = 1$ kpc. The other parameters of the dwarf vary from simulation to simulation and are given in Table 2.

N-BODY CODE

Our N -body code is based on the Poisson solver described by Bontekoe (1988). Specifically, the particle positions are used to evaluate the density on a spherical grid. Then the density within each spherical shell is expanded in spherical harmonics, with harmonics up to $l = 8$ included. This done, the potential at any point can be obtained from BT eq. (2-122). Our code differs from that of Bontekoe in the following

Table 1. Parameters of the model Galaxy

$v_c/\text{km s}^{-1}$	r_c/kpc	r_0/kpc	r_∞/kpc	M/M_\odot
181	1	200	1000	2.5×10^{12}

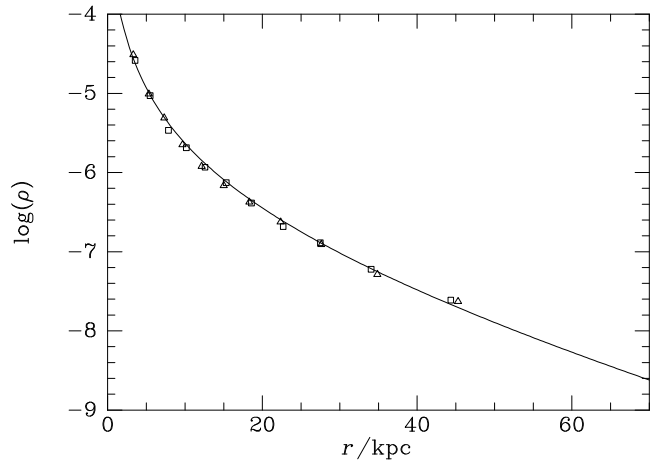
**Figure 1.** The circular-speed curve of the Milky Way and its decomposition into contributions from the disc and halo.

ways.

- Both the angular and the radial grids are adaptive. The radial grid points move so that roughly equal numbers of particles lie in each interval of the radial grid. Within each radial bin, a grid in colatitude θ is established that has roughly equal numbers of particles in each bin, and within each of these bins a grid in azimuth ϕ is established that has equal numbers of particles in each bin.
- There are separate grids for particles belonging to the Galaxy and the Dwarf: the Galaxy's grid has 100 radial points, 24 in θ and 48 in ϕ ; the corresponding numbers for the Dwarf's grid are 12, 12, and 24. At each time-step, the mass distribution due to Galaxy particles is determined on the Galaxy grid. The corresponding potential is then found and used to calculate the forces that the Galaxy imposes on each Dwarf particle. Then the mass of the Dwarf particles is added to the Galaxy grid, the potential redetermined and used to calculate the forces experienced by Galaxy particles. Finally, the mass distribution due to Dwarf particles is determined on the Dwarf grid, the corresponding potential found and used to calculate the forces on Dwarf particles from Dwarf particles.
- The algorithm of Quinn et al (1997) is used to advance the particles with timesteps of length $2^n \Delta_{\min}$, where $n = 0, 1, \dots, 4$.

As a simulation proceeds, particles are stripped from the Dwarf and one needs a method of identifying the particles that remain bound to the Dwarf. The extent, r_t , of the Dwarf is the radius of the largest sphere, centred the last position of the Dwarf's centre, within which the mean density of all particles, Dwarf and Galactic, exceeds the mean density of the Galaxy within the Galactocentric sphere that touches the centre of the Dwarf. The new position and velocity of the Dwarf are the mean position and velocity of the Dwarf particles that lie within the Dwarf's sphere.

The simulations represent the Galaxy with 300 000 particles and the Dwarf with $12000(M_D/10^{11} M_\odot)$ particles.

**Figure 2.** An initial density profile of the Dwarf (a) as an analytic function (curve), (b) as initially sampled (triangles), and (c) after 2.1 Gyr (squares).

Tests

Over 11 Gyr, which is 170 times the central free-fall time $(G\rho)^{-1/2}$ of the Dwarf, the total energy in the simulation changes by $\lesssim 1.7$ percent.

In the absence of potential softening and tidal limitation, the initial configuration of the Dwarf would be a self-consistent equilibrium. Fig. 2 shows the degree to which the Dwarf's density profile changes in the first few dynamical times of a simulation. Specifically: the curve shows the analytic density profile [eq. (2)] that we seek to represent; the triangles show the density profile one infers from the initial positions of the particles; the squares show the density profile inferred 2.1 Gyr later. One sees that any change in the density profile is no larger than the errors inherent in Monte-Carlo sampling the underlying analytic profile.

Results

The full curves in Fig. 3 show three possible orbits for the Dwarf. The initial configurations from which these simulations start are specified by columns 2 to 6 and the rows labelled A, F and K of Table 2: column 2 gives the initial mass that one obtains by integrating the initial density profile [eq. (2)] with the values of the characteristic radii given in columns 4 and 5. Column 6 gives the Dwarf's initial Galactocentric radius. Columns 3 and 7 to 9 refer to the semi-analytic calculations described below. All orbits pass over the Galactic poles and start at apocentre moving at 103 km s^{-1} . The full curves in Fig. 4 show how the mass of the Dwarf declines during the simulations. The full curves in Fig. 5 show as a function of time the one-dimensional velocity dispersion of particles that are bound to the Dwarf. At late times the curves become jagged because the number of bound particles becomes small.

SEMI-ANALYTIC MODEL

In the semi-analytic model we consider the Dwarf to be a particle of variable mass that moves in a fixed potential and

Table 2. Parameters of the orbits. Orbits with upper-case labels in column 1 have been followed with N -body simulations in addition to the semi-analytic model.

Orbit	$\frac{M_{D\infty}}{10^{10} M_{\odot}}$	$\frac{M_D(0)}{10^{10} M_{\odot}}$	$\frac{r_{D0}}{\text{kpc}}$	$\frac{r_{D\infty}}{\text{kpc}}$	$\frac{R_D(0)}{\text{kpc}}$	$\frac{t_{\text{sink}}}{\text{Gyr}}$	$\frac{M_D(t_{\text{sink}})}{10^9 M_{\odot}}$	$\frac{\sigma_D(t_{\text{sink}})}{\text{km s}^{-1}}$
A	10	10	20	70	250	11.1	2.0	23.4
b	10	9.8	25	80	250	13.4	1.1	18.6
c	10	9.9	20	70	225	8.9	2.9	26.1
d	10	9.7	25	80	225	10.9	1.7	21.7
e	10	9.4	25	80	200	8.6	1.9	22.8
F	10	8.8	30	100	200	10.6	1.1	18.8
g	9	8.4	25	80	200	9.9	1.8	21.9
h	7	6.4	25	80	200	14.1	1.0	17.9
i	7	6.7	20	70	200	10.8	1.8	22.0
j	7	6.3	20	70	150	5.9	3.1	27.0
K	5	4.4	20	70	150	9.9	1.8	21.9
l	5	3.7	20	70	100	4.5	3.3	27.9
m	3	2.0	20	70	100	10.1	1.7	21.4
n	3	1.5	20	70	60	3.5	3.0	26.8
o	1.4	0.55	20	70	60	10.5	0.95	17.3

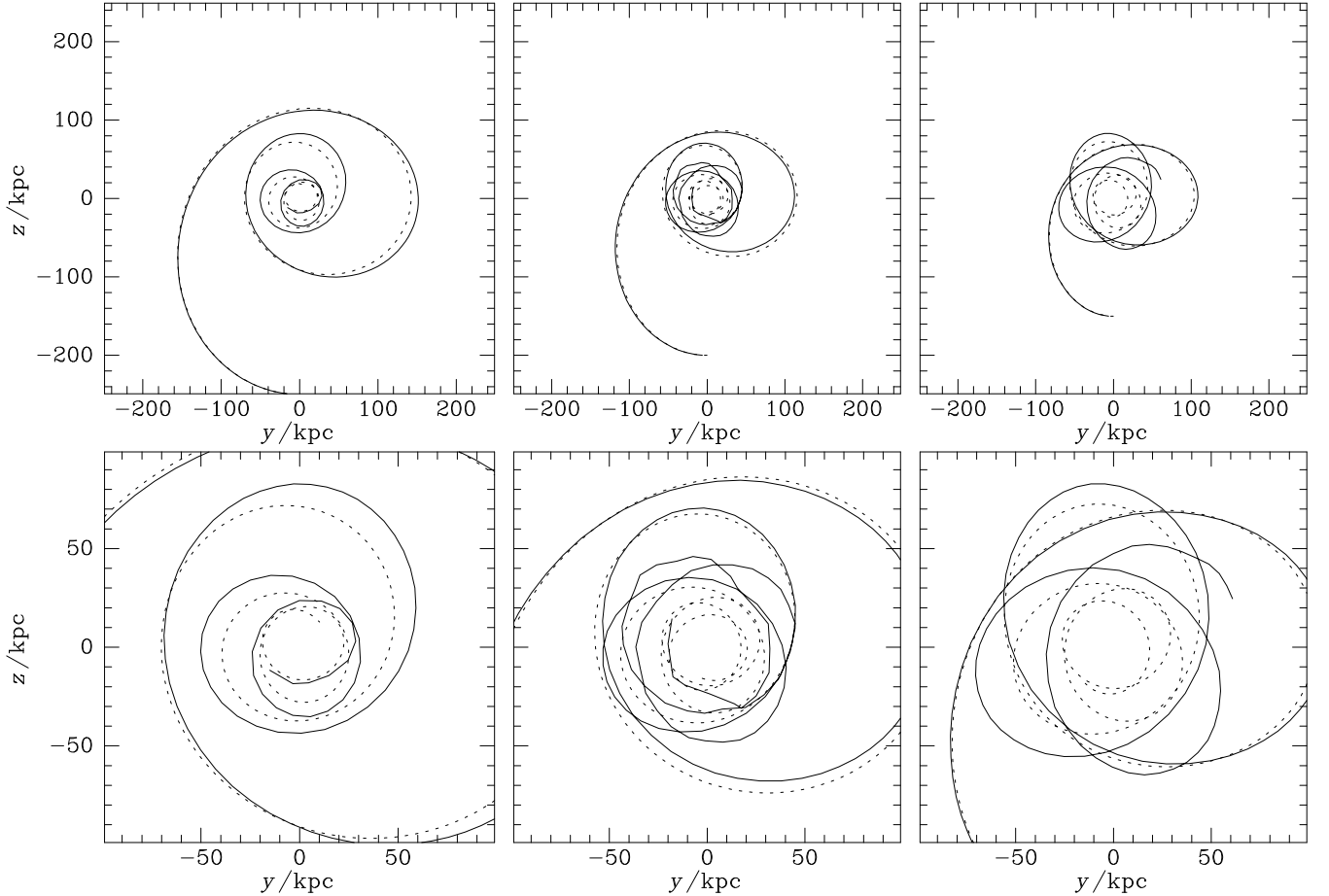


Figure 3. Orbits obtained by full N -body simulation (full curves) and ones obtained with the semi-analytic approximation (dashed curves). The lower three panels show, on an enlarged scale, the central region of the orbit above.

suffers drag as a consequence of dynamical friction. The equation of motion to be integrated for the Dwarf is [BT eq. (7-18)]

$$\frac{d\mathbf{v}}{dt} = -\nabla\Phi_G(r) - 4\pi \ln \Lambda \frac{G^2 \rho_G M_D}{v^3} \left[\text{erf}(X) - \frac{2X}{\sqrt{\pi}} e^{-X^2} \right] \mathbf{v}, \quad (3)$$

where Φ_G is the Galactic potential and $\sqrt{2}X = v/\sigma$ is the ratio of the Dwarf's speed to the one-dimensional velocity dispersion within the Galactic halo at the Dwarf's location. For simplicity, we take Φ_G to be spherically symmetric. The current mass of the Dwarf, M_D , is determined as follows. We

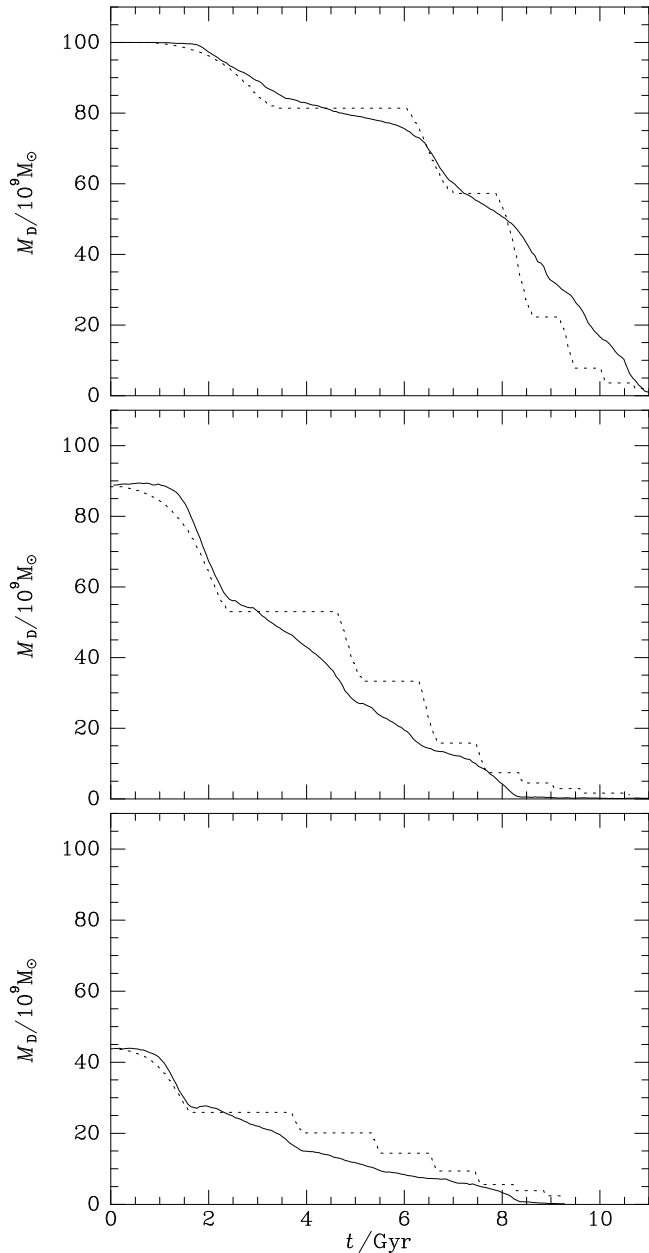


Figure 4. M_D as a function of t for the orbits shown in Fig. 3 from N -body simulations (full curves) and from the semi-analytic model (dashed curves). From top to bottom the panels correspond to the panels from left to right in Fig. 3.

define

$$M_D(r_t, t) = 4\pi D(t) \int_0^{r_t} dr r^2 \rho_D(r, 0), \quad (4a)$$

where $\rho_D(r, 0)$ is the Dwarf's initial density profile [eq. (2)] and

$$D(t) = \frac{\tanh[\beta r_t(t)/r_t(0)]}{\tanh(\beta)} \quad (4b)$$

is a “dilution function” that takes into account the tendency of tidal stripping to decrease the density even inside the tidal radius because some tidally stripped stars initially spent time at small radii. β is a parameter that controls the speed with which the Dwarf is torn apart: if β is large, the

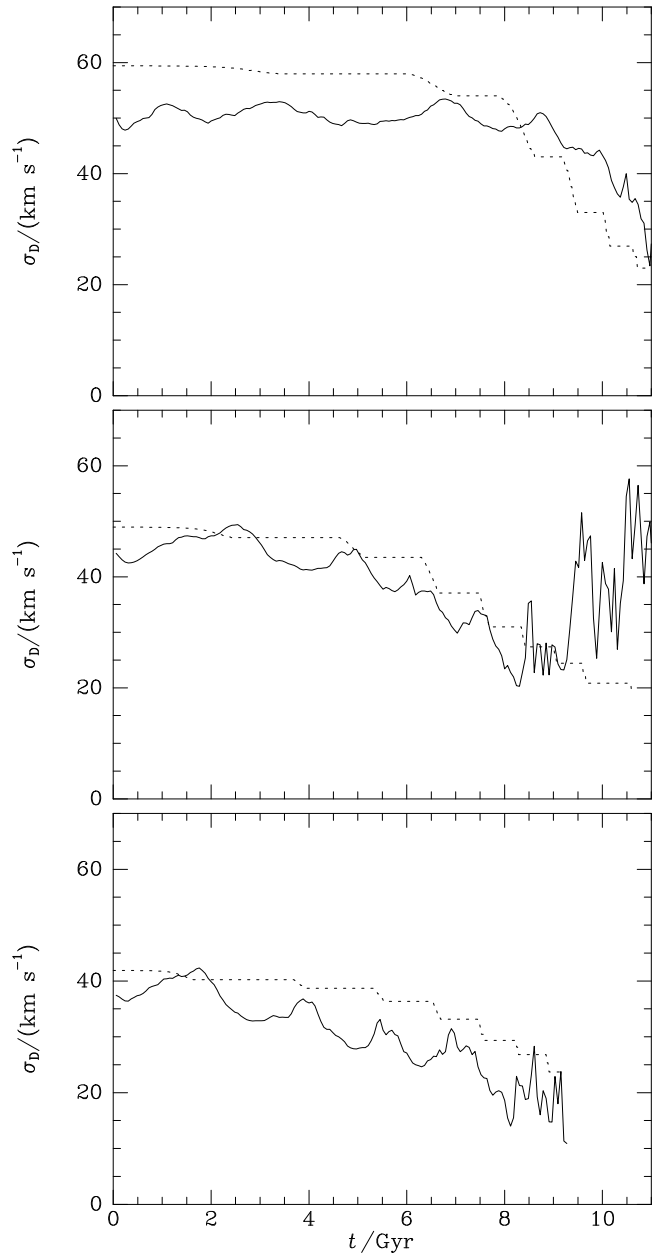


Figure 5. σ_{D0} as a function of t for the orbits shown in Fig. 3 from N -body simulations (full curves) and from the semi-analytic model (dashed curves). From top to bottom the panels correspond to the panels from left to right in Fig. 3.

stripping of material has little impact on the inner Dwarf until mass loss from the outside is far advanced. Equation (4a) gives an estimate of the mass of the Dwarf for any assumed value of r_t . The value of r_t is determined at each time-step by finding the radius r'_t that satisfies the usual tidal condition

$$\frac{M_D(r'_t)}{r_t'^3} = \frac{M_G(r - r'_t)}{(r - r'_t)^3} \quad (5)$$

and then setting $r_t = \min(r_t, r'_t)$. Hence, r_t is not permitted to increase as the Dwarf moves from peri- to apo-centre. Were it allowed to increase, equation (4a) would give rise to an unphysical increase in M_D because it neglects the sharp fall in the density that will in reality be encountered outside

the smallest value that r_t has taken along the orbit: mass lost is lost for ever.

The full curves in Fig. 3 show three orbits for the Dwarf that were followed by full N -body simulation. The dashed curves show orbits integrated from the same initial configurations using the semi-analytical model with $\ln \Lambda = 8.5$ and $\beta = 3.7$ in equation (4b). Although the initial conditions corresponding to the panels differ considerably, the semi-analytic model provides a good qualitative fit to all three until the dissolution of the Dwarf is far advanced. The fit is best for the left-hand orbit, in which a very massive Dwarf starts from a large apocentre. This is the case in which the N -body calculation should be most reliable because at any given time there are always more particles in the Dwarf in this simulation than in either of the others. The major shortcoming of the semi-analytic model is that it makes the Dwarf's orbit unrealistically circular at late times (see the lower panels of Fig. 3). This defect arises because Chandrasekhar's dynamical-friction formula (3) makes the drag proportional to the local density, whereas the response to a satellite is in reality global (Hernquist & Weinberg, 1989). In consequence, equation (3) over-emphasizes dragging at pericentre, where energy is relatively more important than angular-momentum loss.

Fig. 4 shows, for the orbits shown in Fig. 3, plots of M_D as a function of t . The full curves are obtained from the N -body simulations, and the dashed curves from the semi-analytic model. Again we see that the semi-analytic model reproduces the N -body data well, especially for the most massive Dwarf. The main difference between the semi-analytic and N -body curves is a tendency for M_D to be constant after each pericentre in the semi-analytic case. Towards the end of each simulation, when there are only ~ 100 particles in the Dwarf, two-body relaxation will artificially hasten the demise of the Dwarf. Hence the tendency of the semi-analytic models to have larger masses at late times than the N -body models is not necessarily a defect of the semi-analytic models.

The dashed curves in Fig. 5 show the velocity dispersion at $r = 1$ kpc, σ_0 , in the semi-analytic models. This was calculated by integrating the Jeans equation for an isotropic spherical system [BT eq. (4-54)] with the density profile set equal to $D\rho_D(r, 0)$ for $r < r_t$ and zero otherwise. Comparison of Figs 4 and 5 shows that this prescription over-estimates the velocity dispersion in the corresponding N -body model when the semi-analytic model over-estimates the model's mass, and vice-versa when the mass is underestimated. Therefore, the velocity-dispersion values returned by the semi-analytic model probably provide fairly reliable guides to the velocity dispersion of the Dwarf, especially at late times, when small-number statistics make the velocity dispersions of the N -body models very uncertain.

Results

Table 2 summarizes a series of orbits computed using the semi-analytic model. The initial conditions are chosen to illustrate the constraints that must be satisfied if the Dwarf is first to reach a galactocentric radius $r = 16$ kpc in a time, t_{sink} , of order 11 Gyr. The column headed $M_{D\infty}$ is the mass one obtains by integrating the density profile (2). The actual initial mass, $M_D(0)$ given in the next column, is usually

somewhat smaller because equations (4) imply that $r_t < r_\infty$ even at the start of the computation. The columns headed r_{D0} and $r_{D\infty}$ give the values for the dwarf of the characteristic radii r_0, r_∞ of equation (2). $R_D(0)$ is the Dwarf's initial Galactocentric radius, t_{sink} is the time at which it first reaches 16 kpc from the Galactic centre, and $M_D(t_{\text{sink}})$ is its mass at that instant. The final column gives the corresponding velocity dispersion 1 kpc from the Dwarf's centre calculated from the Jeans equation and the density profile $D(t_{\text{sink}})\rho(r, 0)$ for $r < r_t$ as described above.

At the start of the first two orbits, the Dwarf contains $10^{11} M_\odot$ and starts from Galactocentric radius $r = 250$ kpc. The orbits differ in the distribution of mass within the Dwarf: at the start of orbit (b) the Dwarf is more extended than at the start of orbit (a). Consequently, the Dwarf is more rapidly stripped on orbit (b), suffers less dynamical friction, and takes longer to reach the inner Galaxy. At the end of each orbit the Dwarf has been stripped down to $\lesssim 2 \times 10^9 M_\odot$, a mere 2 percent of its initial mass. When 300 000 particles are used to represent the Galactic halo, this mass corresponds to $\lesssim 240$ particles in the Dwarf.

Orbit (c) starts from the same configuration as orbit (a), but at a smaller initial radius, $r = 225$ kpc. Consequently, it reaches $r = 16$ kpc sooner: after $t_{\text{sink}} = 9$ Gyr. If the Dwarf is more extended, $r = 16$ kpc is reached at a later time, as on orbit (d). Orbits (e) and (f) show a similar progression as one moves in to an initial Galactocentric radius $r = 200$ kpc.

Orbit (g) shows that the time required to reach 16 kpc from 200 kpc can be decreased by making the Dwarf more compact, even though of a lower mass. Orbit (h) shows the effect of reducing the mass while holding constant the shape of the density profile: a 27 percent decrease in the mass increases t_{sink} by 35 percent. Orbit (i) reaches $r = 16$ kpc from $r = 200$ kpc in the target time. Orbits (j) to (o) indicate the initial mass and shape required to reach $r = 16$ kpc from $r = 150$ to 60 kpc in the target time.

A constraint on possible orbits is provided by the measured velocity dispersion of the Dwarf's stars: $\sigma_0 = (11 \pm 0.7) \text{ km s}^{-1}$ (Ibata et al. 1997). This may be compared with the velocity dispersions calculated from the semi-analytic model as described at the end of the previous subsection, which are listed in the last column of Table 2. It is striking that although the initial mass declines by a factor ~ 20 from top to bottom through the table, the final velocity dispersion lies in the range 19.4 to 24 km s^{-1} for models in which $t_{\text{sink}} = 10 \pm 1$ Gyr. Two effects must contribute to the significant difference between this number and the smaller observational value. Most obviously, the model value refers to all the Dwarf's material, which is predominantly dark. Since the dark matter is more extended, its central velocity dispersion must be larger than the value measured for the luminous matter. A second effect is velocity anisotropy: the model assumes velocity isotropy, which almost certainly does not hold. The measured value is for a line-of-sight almost perpendicular to the Dwarf's long axis, which by the tensor virial theorem should be lower than the line-of-sight value for the corresponding isotropic model. If both of these effects caused the observational value to be smaller than the calculated value by a factor ~ 1.2 , the difference between theory and observation would be fully accounted for. It is plausible that the factors are of this order, though only substantially more sophisticated modelling could reliably deter-

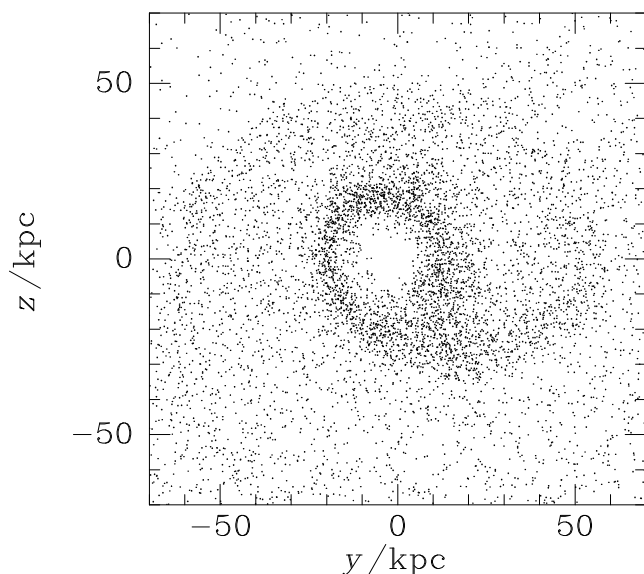


Figure 6. The distribution of Dwarf particles projected onto the plane perpendicular to the Dwarf's orbit.

mine them.

CONCLUSIONS

We have modelled the orbital decay of the Sgr Dwarf under the assumption that the Galactic halo extends to 250 kpc. A mixture of N -body simulations and semi-analytic modelling suggests that the present configuration of the Dwarf is consistent with a wide variety of orbital histories. At one extreme the Dwarf starts out with a mass $\sim 10^{11} M_{\odot}$ at a Galactocentric radius $\gtrsim 200$ kpc. At the other extreme it starts out with a mass $\sim 1.2 \times 10^9 M_{\odot}$ at a radius ~ 60 kpc, as suggested by Ibata & Lewis (1998). The larger the initial Galactocentric distance of the Dwarf, the more massive the Dwarf must have been initially. The final velocity dispersion of the Dwarf is remarkably insensitive to the Dwarf's history, because as the initial distance of the Dwarf is increased, its dark halo has to be extended at an approximately constant velocity dispersion, in order to maintain an appropriate rate of orbital decay and tidal stripping by the Galactic potential, which has nearly constant velocity dispersion by construction.

If the Galaxy has stripped $\gtrsim 10^{10} M_{\odot}$ from the Dwarf, the stripped material should form a complete ring around the sky – see Fig. 6. Unfortunately, the great majority of the mass plotted is dark and not directly observable. Luminous matter was originally confined to the centre of the Dwarf and will have been stripped in quantity only recently. Hence it will be less uniformly spread over the sky than the dark matter.

In general dark matter can only be detected through its gravitational field. Fortunately, we have a sensitive gravitational field detector in place: the outer Galactic disk. We hope soon to report on how the Galaxy's outer HI disk responds to the time-dependent gravitational field that is generated by both the Dwarf and the Magellanic Clouds. It is already apparent that the more massive Dwarf models generate distortions of the disk that are comparable in magnitude to the observed Galactic warp. What is still unclear

is whether the Dwarf and Clouds can between them explain the particular morphology of the Galactic warp.

REFERENCES

- Binney J.J., Tremaine S.D., 1987, 'Galactic Dynamics', Princeton University Press, Princeton (BT)
- Bontekoe T.R., 1988, Ph.D. thesis Groningen University
- Dehnen W., & Binney J.J., 1997, MNRAS, 294, 429
- Gómez-Flechoso M.A., Fux R., Martinet L., 1999, astro-ph/9904263
- Hernquist L., Weinberg M., 1989, MNRAS, 238, 407
- Ibata R.A., Gilmore G., Irwin M.J., 1994, Nature 370, 194
- Ibata R.A., Lewis G.F., 1998, ApJ, 500, 57
- Ibata R.A., Wyse F.G., Gilmore G., Irwin M.J., Suntzeff M.B., 1997, AJ, 113, 634
- Jiang I.-G., Binney J.J., 1999, MNRAS, 303, L7
- Johnston K.V., Spergel D.N., Hernquist L., 1995, ApJ, 451, 598
- Quinn T.R., Katz N., Stadel J., Lake G., 1997, astro-ph/9710043
- Schmoldt I.M., Saha P., 1998, AJ, 115, 2231
- Velásquez H., White S.D.M., 1995, MNRAS, 275, L23
- Zhao H.-S., 1998, ApJ, 500, L149

This paper has been produced using the Blackwell Scientific Publications \TeX macros.